Plasmonic blackbody: Almost complete absorption of light in nanostructured metallic coatings

V. G. Kravets, F. Schedin, and A. N. Grigorenko
Department of Physics, University of Manchester, M13 9PL Manchester, United Kingdom
(Received 10 May 2008; revised manuscript received 24 July 2008; published 6 November 2008)

We have experimentally demonstrated blackbodylike behavior in a thin nanostructured metallic layer shaped in the form of a composite deep diffraction grating. This behavior is recorded over a wide optical wavelength range (240–550 nm) and for a broad range of angles of light incidence (0–75°) for samples with metal thickness of just 90 nm. The strong absorption at a level of 97–99% is observed for one light polarization and is attributed to excitation of localized plasmons coupled to incident light waves. We show that the studied structures exhibit anomalies which consist in disappearance of reflection for both *p*- and *s*-polarized light at corresponding "Brewster" angles. An effective-medium approach provides a satisfactory qualitative description of the reflection and transmission spectra in our samples and confirms their blackbody behavior.

DOI: 10.1103/PhysRevB.78.205405 PACS number(s): 78.67.−n, 71.45.Gm, 73.22.Lp, 78.20.Ci

I. INTRODUCTION

By Kirchhoff's definition, the blackbody is an object that absorbs all light that falls on it. Perfect blackbody absorbs electromagnetic radiation of any wavelength and does not produce reflected or transmitted light under any kind of illumination. Blackbody surfaces are of increasing importance in many fields of science and modern technologies. It has been shown recently that thermal emitters fabricated from polar materials, which possess blackbodylike behaviors, can be used as effective directional thermal infrared sources coherent over a large number of wavelengths.[1] Blackbody surfaces are often used as extremely low reflectance coatings in optical instruments and sensors with dramatically improved efficiency and precision.[2,3] One of the most promising application of the blackbody coatings is in the field of photothermal and photoelectrical conversions of the solar energy where they could considerably increase the effectiveness of solar cells.[4–6]

A perfect blackbody is an ideal object[7,8] that should totally absorb light of all wavelengths and for all incident angles. As a result, only few objects are able to demonstrate blackbodylike behaviors. Currently, "blackbodies" are made either from graphite[9] or from cavities covered with black paint often containing graphite particles (soot).[10] Recently, a theoretical calculation showed an extremely low index of refraction ($n=1.01-1.10$) for low-density vertically aligned carbon nanotube arrays.[11,12] Using aligned nanotube composites, scientists produced blackbody with ultralow diffused reflectance in visible spectrum.[13] However, the aligned nanotube coatings consist from very thick (~ 100 μm) and extremely fragile building blocks, which can degrade the advantage of their applications.

The promising candidates for a design of robust blackbody absorbing layers are plasmonic photonic crystal structures. While smooth metal surfaces reflect most of incident visible light and cannot be used as blackbody surfaces, the optical properties of a metallic film can be significantly altered by its nanostructuring that allows one to "manufacture" a desired index of refraction and achieve extraordinary optical properties. Collective electronic excitations called plasmons—both propagating and localized—a Bragg reflection, and a modification of density of states via plasmonic band gap are the main physical mechanisms for achieving strong absorption of light in periodic metallic structures.[14–18]

It is well established that shallow metallic gratings can act as perfect absorbers. However, the total light absorption in these gratings occurs only when the Bragg or Rayleigh resonances take place and therefore is observed in narrow wavelength bands.[18,19] The resonance conditions originate from matching of wave vectors of incident light; Bloch waves generated by the periodic structure of the grating and propagating plasmons;[16,19] the total light absorption is attributed to the incoming light being transformed into propagating surface plasmons which convert the energy of light into thermal energy. Narrow wavelength and incident angle ranges of the total absorption observed in shallow metallic gratings make them unsuitable for a blackbody fabrication.

The situation is different for metallic gratings with a deep surface modulation that could break continuity of a metallic film. In this case strong light absorption happens through the excitation of localized plasmons (which are easily excited by incident light) and therefore the conditions for observation of strong absorption and blackbodylike behavior in this case are more relaxed. A deep subwavelength metallic grating can be considered as an array of metallic stripes and the "effective" refractive index of the whole structure can be tuned to a value that would guarantee strong light absorption. As a result, one may hope to fabricate the refractory metal coatings and absorbing covering layers using nanostructured metallic films with deep height modulations.

In this work we experimentally demonstrate plasmonic blackbody based on deep diffraction gratings made of extremely thin (90 nm) and robust gold films deposited on poly-methyl-methacrylate (PMMA) nanostripes. By blackbody in this paper we imply an object which strongly absorbs light in a wide spectral and angle range demonstrating blackbodylike behavior. We measure reflectance, transmittance, and ellipsometry spectra for the samples of two orientations (gold stripes perpendicular plane of incidence and gold stripes parallel to the plane of incidence) and for two light polarizations (*p*-polarized and *s*-polarized light). We show that optical spectra of our structures can be tuned by adjusting the geometry of the gratings. For gold nanostructures, 97–99% of light absorption is observed in a wave-

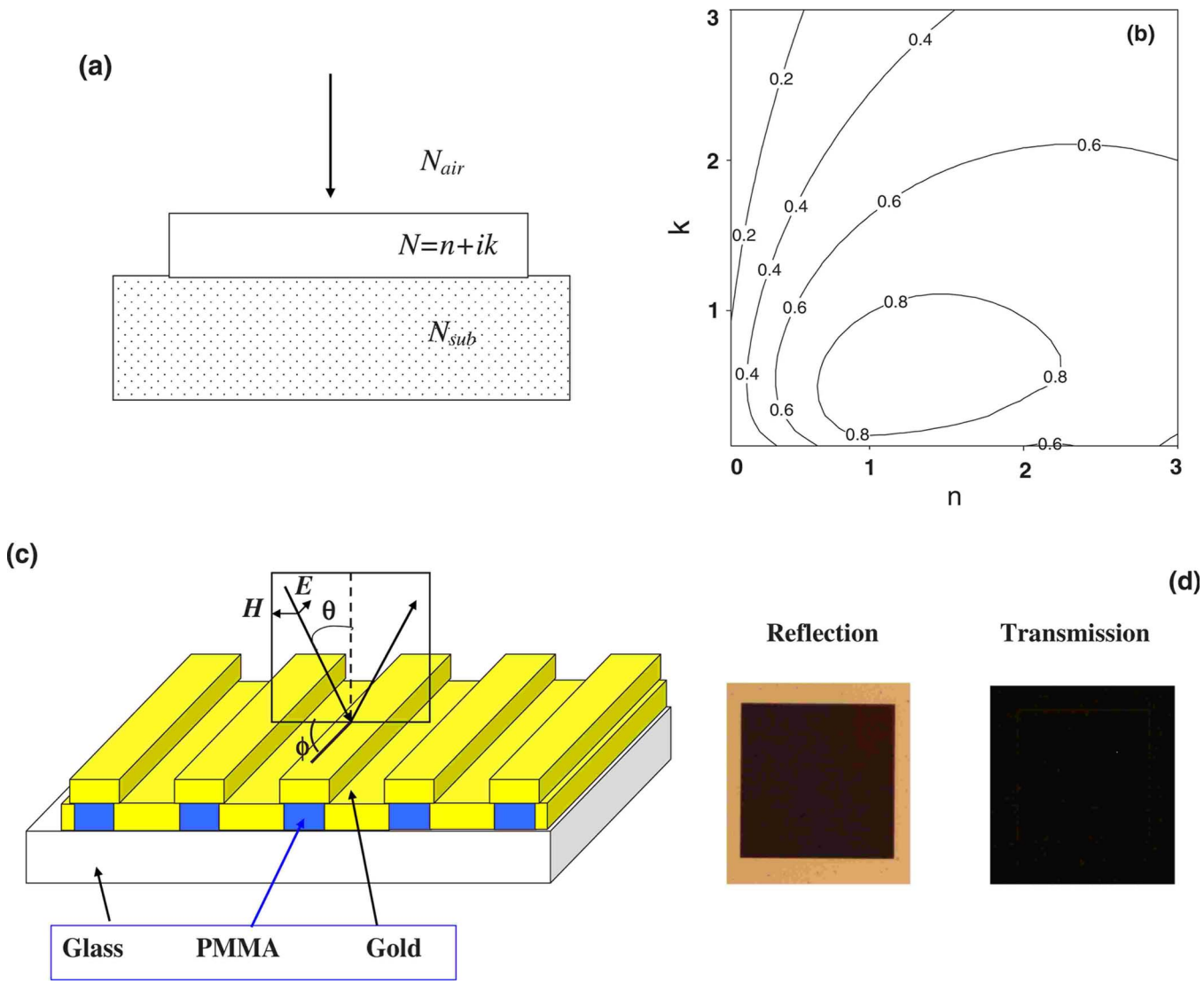

FIG. 1. (Color online) Schematics of plasmonic blackbody. (a) Schematic view of the coating layer on a substrate. (b) A contour plot of the absorption coefficient in n-k coordinates. (c) The geometry of a 1D subwavelength grating. (d) Optical microscopy images in reflected and transmitted light of the best structure.

length range of 240–550 nm for the large range of the incident angles (0–75°) for the light with electric-field vector perpendicular to the grating stripes. The light with electric vector directed parallel to the grating stripes was reflected with the same efficiency as that from a plain gold film. As a result, our structures can provide a high polarization separation ratio for reflected light in a wide incident angle range for ultraviolet and visible light, and therefore, can be used as a reflection polarizer. We experimentally found that the absence of reflection (which we refer to as Brewster-type effect) can be realized for both p- and s-polarized light simultaneously for the studied structures.

The paper is organized as follows. In Sec. I we discuss the effective optical constants of thin blackbody coatings and the sample design. In Sec. II we describe fabrication procedures and experimental methods used in our work. In Sec. III we discuss our experimental results, which include the reflection, transmission spectra for different light polarizations, and sample orientations and demonstrate the blackbody behavior in our samples. In Sec. IV we present effective-medium theory that gives qualitative description of our experiments. Finally, the conclusion is given.

II. SAMPLE DESIGN

First, we briefly describe the main idea under the plasmonic blackbody design. Let us consider a homogeneous thin coating layer of thickness d of the refractive index $N=n+ik$ that covers a surface of materials with the index of refraction N_{sub} [see Fig. 1(a)]. (For the sake of simplicity we assume that the materials are in air with an index of refraction $N_{air}=1$.) To produce a blackbody we search for the coating layer with the best absorbing characteristics. The transmission and reflection of this system are given by the Fresnel coefficients.[20,21] A simple examination of the Fresnel coefficients shows that for any fixed thickness d there exists a range of the indices of refraction of the covering layer N which would guarantee the maximal light absorption. For

example, the combination of $n \approx 1$ and small k provides almost total absorption of light in the covering layer when d is much larger than the wavelength of the light, λ. (The fact that $n \approx N_{\text{air}}$ guarantees the absence of reflection from the first interface and the imaginary part of the refractive index assures the total light absorption in the covering layer provided $2\pi kd/\lambda \gg 1$.) This combination was used for production of a blackbody based on aligned nanotubes.[13] As we explained above, the disadvantages of this approach are relatively large thickness of the covering layer and its fragility ($n \approx 1$ implies an extremely porous structure for the layer).

Remarkably, the absorption of a coating layer in visible light can be high even when the layer is very thin, just a few hundred nanometers. Figure 1(b) shows the absorption coefficient of the coating layer of the thickness $d=140$ nm as a function of n and k. It is clear that one obtain absorption at the level of 90% in the absorbing layer at the $n=1.3$ and $k=0.5$ for $\lambda=400$ nm. Therefore, the layer with the index of refraction $N \approx 1.3+0.5i$ would guarantee a very strong absorption of visible light in the system shown in Fig. 1(a). Such an index of refraction is difficult to find in *natural* materials. However, the developing field of metamaterials allows one to engineer the optical materials with desired index of refraction. For example, the optical constants of a nanostructured metal can be governed by the geometry of the structuring and can be tuned to the values that would guarantee a strong absorption in the covering layer.

We show below that effective constant of deep gold gratings deposited on PMMA relief can be made equal to the optimal values for the maximal light absorption in the coating layer. For this reason, we have investigated a structure shown in Fig. 1(c) as a prospective design for the blackbody covering. Figure 1(d) demonstrates the main experimental result of our work—the optical photographs of our best structures taken in reflection and transmission, which show the blackbodylike behavior of the nanostructured metal in visible light (the sample appears to be completely black in transmission and reflection). Our results suggest that the nanostructured metal of the thickness of about 100 nm can be used as very effective antireflecting and absorbing coatings (refractory metal coatings), which guarantee strong light absorption in a large spectral range in the visible spectrum.

III. EXPERIMENTAL DETAILS

Deep gold composite diffraction gratings were fabricated on glass slides by electron-beam lithography and metal evaporation. The glass substrates were coated with 5 nm of chromium in order to minimize charging during the fabrication. PMMA of the total thickness of 120 nm was spun on the substrate and was baked. The nanostripe arrays were exposed by electron-beam lithography and the samples were developed resulting in one-dimensional (1D) array of PMMA stripes of width b with the array constant a. Thermal evaporation has been used to deposit 5 nm of Cr and 90 nm of Au onto the developed structures. This procedure resulted in a gold film arranged in flat-shaped gold stripes of width b formed on the top of the PMMA relief and gold stripes of width a-b formed on the glass substrate in between PMMA stripes. Both types of gold stripes produced a square 1D array with an identical grating constant of $a=320$ nm. The whole sample has size of 200×200 μm^2. Figure 1(c) depicts the schematics of the sample design and shows the scanning electron micrograph of the sample taken under a tilted angle (Fig. 2). The width of the stripes has been varied between $b \sim 100$ nm and ~ 170 nm, as determined by scanning electron microscopy (SEM) (Fig. 2).

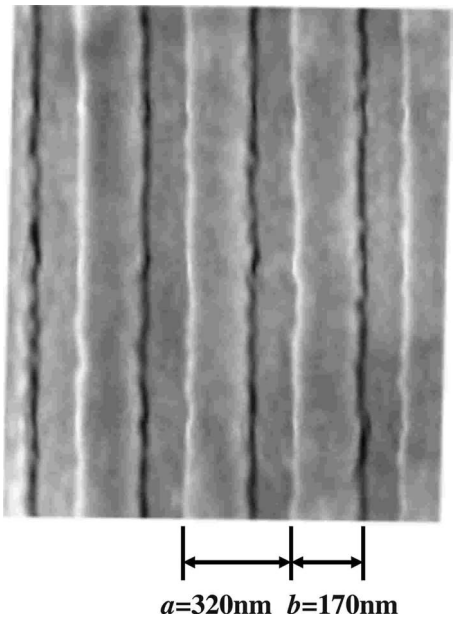

FIG. 2. A SEM image of one of the studied gold nanostripes taken under a tilted angle.

In 1D periodic gold nanostripe arrays there is a marked distinction between the two orthogonal directions within the plane of the stripes [see Fig. 1(c)]. One direction is characterized by the existence of discrete translation symmetry. The other direction supports continuous translational symmetry. The two types of translation symmetry lead to drastically different optical response of the stripes to the light of different polarizations and planes of incidence. For this reason, we studied optical properties of our samples for two different orientations of the light polarization and two different orientations of the stripe arrays. Our measurements confirmed that the relative configuration between polarizations of light and periodicity of stripe strongly influence optical response of the studied structures.

The ellipsometric spectra and polarized reflection spectra of the gold stripes have been measured by the focused beam M-2000F spectroscopic ellipsometer (J. A. Woollam, Inc.) which provides a small measurement spot (down to 30 μm). This instrument is ideal for our investigations where the measurement area is small. To determine the dispersion of the modes associated with the periodical structure of stripes we recorded a pair of ellipsometric parameters,[20] Ψ (restored angle) and Δ (phase shift), in the wavelength range from 250 to 1000 nm. Ψ and Δ are given in terms of the complex reflection coefficients, r_p and r_s, as $r_p/r_s=\tan\Psi \times \exp(i\Delta)$ (see Ref. 20). The ellipsometric parameters have been measured for incidence polar angles θ ranging from 45° to 74°. The samples were rotated along the vertical axis to provide

the azimuth angle ϕ variations [see Fig. 1(c)]. Two configurations of the azimuth angle, $\phi=0°$ and 90°, will be discussed for which the plane of incidence is oriented either along the stripes of the array or perpendicular to them, respectively. The reflectance measurements were also performed for the same two values of ϕ. The reflectivity spectra were acquired for two settings of polarizations of incident light: p polarization (electric field in the plane of incidence) and s polarization (electric field perpendicular to the plane of incidence).

Optical transmission spectra were collected with a visible—near-infrared Ocean Optics USB2000 spectrometer (with the spectral range of 400–830 nm). A xenon lamp was used as the light source. The light passed through a polarizer and then was focused by objective on the surface of sample to a spot of approximately 50 μm. The sample was mounted on a rotation stage. The transmitted light was collected using an optical fiber coupled to the spectrometer (200 μm core). The angle of incidence was varied from 0° to 60°. The transmission spectra were also measured for both p- and s-polarized illuminations. The transmission spectra presented here are found by normalizing spectra measured through the gold nanostripes by spectra measured through the air.

IV. RESULTS AND DISCUSSION

We now discuss the optical response of the studied deep gold composite diffraction grating (which we will refer to as nanostripes) and, more importantly, we show that the reflection and transmission can show low values in a large wavelength range ($\leq$1% for some angles of incidence). Figures 3(a) and 3(b) illustrate p- and s-polarized reflectivity spectra measured at different incident angles ($45° \leq \theta \leq 74°$ in steps of 4°) for gold stripes of width $b \sim 150$ nm, the grating constant $a=320$ nm, and the azimuth angle $\phi=90°$. For all incident angles the reflectivity is close to zero for p-polarized light at the wavelength range of 240–550 nm. A more detailed analysis shows that for p-polarized light angular dependence of spectra $R_p(\lambda)$ exhibits minimum in the range $\lambda \sim 520-620$ nm and then rapidly increases with increasing the incident wavelength. These spectra reach maximum in the region $\lambda \sim 550-650$ nm, and after that $R_p(\lambda)$ slowly decreases with increasing wavelength [Fig. 3(a)]. The s-polarization spectra $R_s(\lambda)$ do not show significant changes for examined structure and look similar to the reflection spectra observed for homogeneous thick gold films [Fig. 3(b)]. Inset of Fig. 3(b) shows the reflection spectra for p- and s-polarized light measured at the normal angle of incidence ($\theta=0°$) using reflection spectrometer.[14] We see that the reflection from our samples is very small for the p-polarized light in a wavelength range of 370–530 nm for the normal angle of incidence as well.

Figures 3(c) and 3(d) show the transmission spectra of the gold nanostripes for p- and s-polarized light, respectively, for the same azimuth angle $\phi=90°$. There are negligible changes in the intensity of transmission light for all spectral region, and spectra for both polarizations are similar. The optical transmission for both polarizations leads to an extremely low value less than 0.5%. For angles of incidence 45° and 60° the

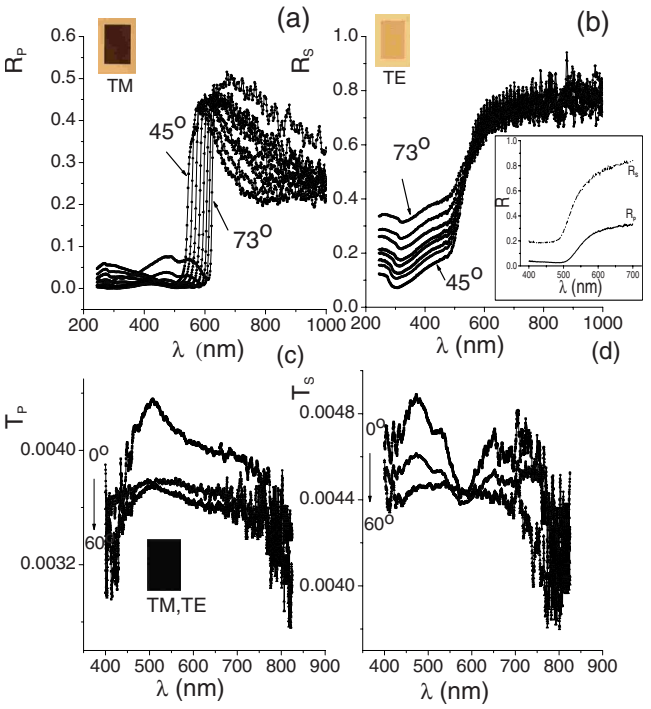

FIG. 3. (Color online) Optical properties of the nanostripe array with $a=320$ nm and $b=150$ nm measured for the azimuth angle $\phi=90°$. The reflection spectra for the light of (a) p and (b) s polarizations. The transmission spectra for the light of (c) p and (d) s polarizations. Insets show the polarization-contrast optical microscopy images for [(a) and (b)] reflected and (c) transmitted light. Second inset of Fig. 3(b) shows the reflection spectra for p- and s-polarized light at normal incidence.

level of intensity for the transmitted light in the whole spectral range of 400–1000 nm is close to the experimental noise. Small broad peaks in transmission occur at $\lambda \sim 500$ nm for the normal angle of incidence [Figs. 3(c) and 3(d)].

For all angles of incidence (at $\phi=90°$) we observed pronounced reflectivity plateau with values of $R_p(\lambda)$ as low as 1–3% in the spectral range 240–550 nm. Transmission experiments revealed that within plateau only 0.5% of the incident light is transmitted through the gold stripes. Using Kirchhoff's rule [the sum of the transmittance $T(\lambda)$, reflectance $R_p(\lambda)$, and absorbance $A(\lambda)$ should be equal to 1 in the absence of scattering and diffraction], we conclude that the coefficient of absorption for the studied grating was about 97% in the frequency range of 240–550 nm. The contribution of diffraction was negligible in the region of $a[1+\cos(\theta)] < \lambda$ (see Ref. 21 chapter 8) and was below 10% for other cases (this estimate was obtained using a theoretical approach suggested in Ref. 22). Therefore, the gold nanostripes behave as an effective broadband absorbing coating mimicking the behavior of a blackbody in a wide spectral range that covers a large portion of visible spectra important for the operation of solar cells and in a wide range of incident angles.

The inset of Fig. 3 shows the polarization-contrast microscopy images of our samples, which confirm the blackness of our object. In experiment the electric field of the white light was set to be either perpendicular to the stripes,

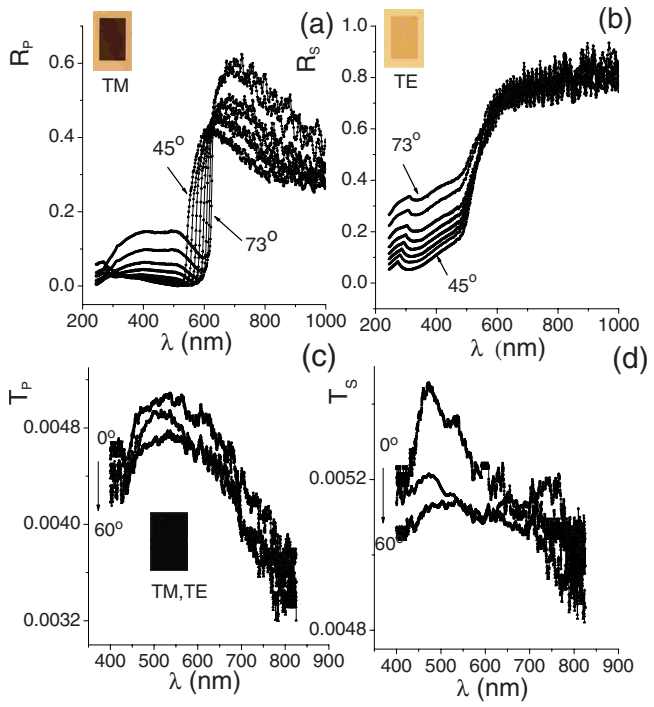

FIG. 4. (Color online) Optical properties of the nanostripe array with $a=320$ nm and $b=170$ nm measured for the azimuth angle $\phi=90°$. The reflection spectra for the light of (a) p and (b) s polarizations. The transmission spectra for the light of (c) p and (d) s polarizations. Insets show the polarization-contrast optical microscopy images for [(a) and (b)] reflected and (c) transmitted light.

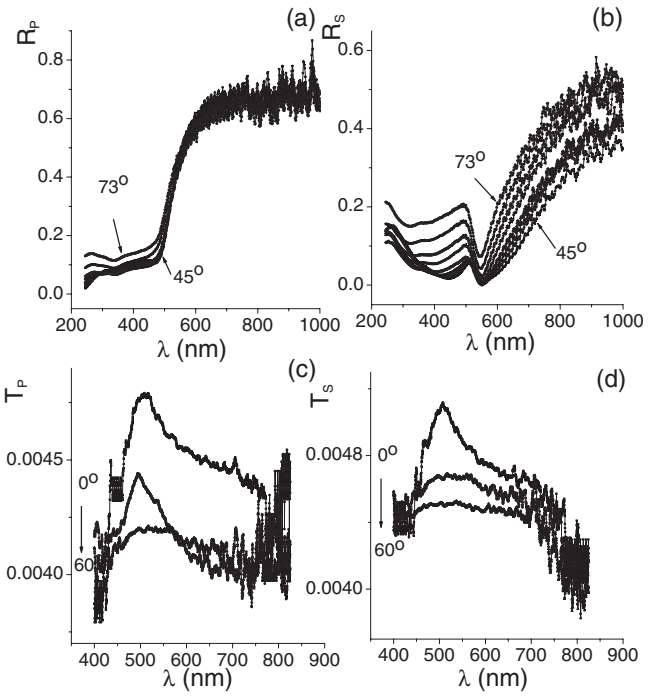

FIG. 5. Optical properties of the nanostripe array with $a=320$ nm and $b=150$ nm measured for the azimuth angle $\phi=0°$. The reflection spectra for the light of (a) p and (b) s polarizations. The transmission spectra for the light of (c) p and (d) s polarizations.

TM mode of the polarization, or parallel to the stripes, TE mode of polarization. The light transmitted or reflected from the gold nanostripes was collected by an objective and was sent to a charge coupled device (CCD) camera. These polarization-contrast optical images provided a simple and quick way to assess the blackness of the gold nanostripes observed in the TM illumination.

For comparison, we also present the optical characteristics of the nanostripe array with a nonoptimized value of $b\sim170$ nm (and the same $a\sim320$ nm and $\phi=90°$). Figure 4 depicts the reflection and transmission spectra measured for p- and s-polarized light. Plots (a) and (c) show again almost blackbody behavior for p-polarized light analogous to that shown in Figs. 3(a) and 3(c). The reflectance value for this configuration of nanostripes is at the level of about 10% in the wavelength range of 240–550 nm. In contrast to the p-polarization results, the s-polarization reflectivity for $\phi=90°$ shows a monotone behavior [Fig. 4(b)]. At the same time we can see that the $T(\lambda)$ spectra are quite similar to the ones presented in Figs. 3(c) and 3(d), which implies that the geometry of the diffracting grating has a small effect on the sample transmission.

Several experiments were carried out in order to cover a broad range of stripes width $b\sim110$, 120, and 130 nm [the spectra of $T(\lambda)$ and $R_p(\lambda)$ are not shown here]. Within this range the magnitude of reflection coefficient R_p at $\phi=90°$ tends to be $\sim5-10\%$ at the wavelengths from 240 to 550 nm, and the transmission T is below 1% for both polarizations. This value is larger than those presented in Figs. 3 and 4. Our measurements showed that the smallest value of $R_p(\lambda)$ is very sensitive to the variations of the width of the gold nanostripes. From the obtained results we can conclude that the changes in the stripe width (the fill factor of the gold in the structures, see below) strongly affect the blackbody behavior. Thus the optimal 1D stripes parameters for the design of blackbody were determined to be filling factor $f=b/a\approx0.5$, and grooves depth $h=90$ nm.

The reflectance measurements were also performed for the second configuration when the stripe lines are parallel to the incident plane, $\phi=0°$ [Fig. 1(c)]. The spectra observed in this configuration (Fig. 5) are completely different to those shown in Figs. 3 and 4. In case of $\phi=0°$ it is the reflection spectra $R_s(\lambda)$ of the gold stripes [see Fig. 5(b)] that display a more complex structure than the reflection for p-polarized light shown in Fig. 5(a). At low incident angles $\theta\leq55°$ the reflectivity $R_s(\lambda)$ for $\phi=0°$ is actually close to the reflection $R_p(\lambda)$ observed for the case of $\phi=90°$, compare Figs. 3(a) and 4(b), while $R_p(\lambda)$ for $\phi=0°$ is analogous to $R_s(\lambda)$ for $\phi=90°$ [and $R(\lambda)$ for a gold film], compare Figs. 3(b) and 4(a). For incident polar angles ($55°\leq\theta\leq74°$) the $R_s(\lambda)$ at $\phi=0°$ shows a pronounced dip at $\lambda\sim530-550$ nm. The spectral position of the dip is shifted toward lower wavelengths when the angle θ increases. The dip in $R_s(\lambda)$ becomes more pronounced, and its magnitude strongly increases with the increase in the incident angle. The magnitude of $R_s(\lambda)$ reaches exactly zero for incident angle of $\theta\sim55°$. Therefore, our structures can show "Brewster effects" (the absence of reflection) for the light of s polarization at $\phi=0°$. For all spectra the amplitude of $R_s(\lambda)$ increases

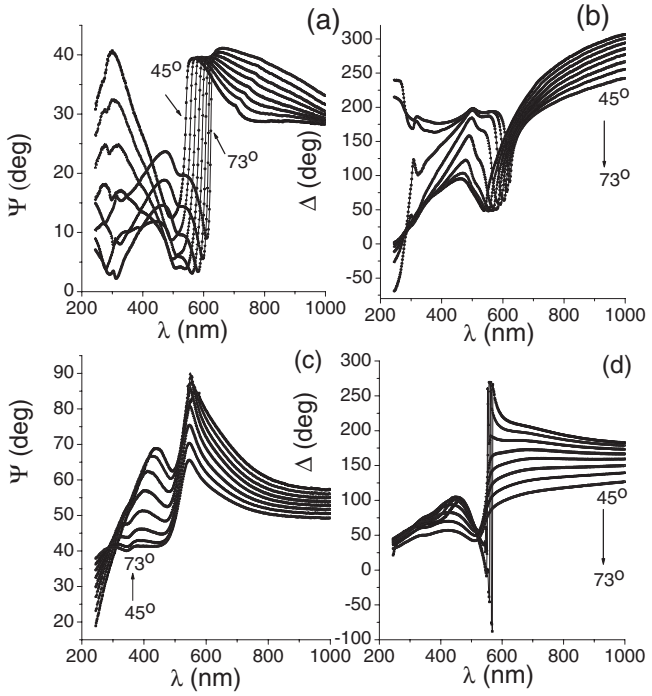

FIG. 6. Spectroscopic ellipsometry for the nanostripe array with $a=320$ nm and $b=150$ nm. The ellipsometric parameters for the azimuth angle $\phi=90°$ (a) Ψ and (b) Δ. The ellipsometric parameters for the azimuth angle $\phi=0°$ (c) Ψ and (d) Δ.

in the spectral region of $\lambda \sim 550-1000$ nm. The spectral behavior of $R_p(\lambda)$ is less complicated, and the reflectivity versus angle as well as wavelength is a monotonous function. The measured transmittance is presented in Figs. 5(c) and 5(d). For comparison, we again tested the samples at different angles of incidence. The transmittance is again very low and its value is consistent with the results presented in Figs. 3(c), 3(d), 4(c), and 4(d).

Now we turn our attention to ellipsometric spectra observed in our structures. We observe significantly different ellipsometric spectra, Ψ and Δ, for the diffracting grating; whether the plane of incidence is parallel ($\phi=0°$) or perpendicular ($\phi=90°$) to the stripes. The ellipsometric spectra shown in Fig. 6 for different angles of incidence are almost identical for wavelengths above 600 nm, whereas they clearly differ from each other in the 240–600 nm wavelength range. This lower wavelength region is therefore the most relevant for the appearance of grating anomalies which determine the shape of ellipsometric functions. It was found that spectral dependences of functions Ψ and Δ are sensitive to the angle of incidence. In the case of $\phi=90°$, two enhancement minima are visible in the curves Ψ and Δ for gold stripes [Figs. 6(a) and 6(b)] which are peaked at wavelengths $\lambda \sim 300$ and $\sim 550-600$ nm. The minima positions are governed by the grating constant a. Similar results were obtained on SiC gratings.[1] Second minimum ($\lambda \sim 550$ nm) is more prominent than the first one. This dip becomes stronger and narrower with an increase in θ from 45° to 74°. It should be noted that the slopes of the Ψ curves in the region 550–600 nm, which corresponds to changes for Ψ from minimal to maximal values, are practically vertical. We found that the wavelengths of the dip for functions Δ are slightly larger than spectral positions of the minima for the corresponding functions of Ψ (Fig. 6). Figure 6(c) shows that the ellipsometric parameter Ψ has a maximum where the *s*-polarized reflection goes through zero. This is unexpected since usually it is the *p*-polarized Fresnel reflection that has a zero reflection at the Brewster angle in the case of a light falling onto interface between two media. The existence of the Brewster-type effect for both *p*- and *s*-polarized reflection waves (Fig. 6) is explained in our case by the fact that our system is a thin nonhomogeneous film on a dielectric substrate for which destructive interference can lead to the absence of reflection for both polarizations. The fact that the reflection coefficient for our sample goes through zero is also confirmed by the spectral properties of ellipsometric function, Δ. Note that the phase shift Δ demonstrates a jump on 180° at the critical angles and at resonance wavelengths even in the case of *s*-polarized reflection [Fig. 6(d)], which is a sign of singularity in reflection.[23]

V. EFFECTIVE-MEDIUM THEORY

A number of different techniques have been used to model optical properties of deep metallic gratings. These include rigorous coupled-wave analysis (RCWA),[24,25] integral equation methods,[22,26–29] discrete dipole approximation,[30] etc. However, the geometry of our gold nanostructures is different from deep rectangular metallic gratings that have been investigated in above-mentioned references. In contrast to deep metallic gratings prepared by plasma etching methods, our structures are produced by a deposition of gold onto a PMMA stripe-relief. For this reason, the geometry of our structures is more complicated and should be described by two gratings (PMMA-gold and gold-air) placed on top of each other with a translational shift. Such a system has not been considered using a rigorous approach before. For this reason, to describe the interaction between the incident light and gold nanostripes we utilize the effective-medium approximation (EMA) and assign a complex effective index of refraction to our structure. For subwavelength diffraction gratings this refractive index can be calculated by using, e.g., Maxwell-Garnett approach.[12,31] It has to be noted that this approach is valid when $a \ll \lambda$. Surprisingly, we found that the EMA approach described below gives a good agreement with our experimental data even when $a \sim \lambda$. Within this theory the effective dielectric constant can be written as a function of the polarizability of an individual stripes $\alpha(\omega)$ and the depolarization factor L_d (describing dipole interaction between stripes) which depend on the polarization of the incident light,[12]

$$\varepsilon_{\text{eff}}(\omega) = 1 + \frac{f\alpha(\omega)}{1 - fL_d\alpha(\omega)}, \tag{1}$$

where $f=b/a$ is the volume fraction occupied by stripes. In this approach the relief structure of gold stripes will be approximated by an anisotropic uniaxial medium characterized by the effective dielectric constants for direction perpendicular ($\varepsilon_\perp$) and parallel to the stripes ($\varepsilon_\parallel$). (Such an approximation works well for thin samples discussed in this paper and

simplifies the calculations considerably.) The perpendicular polarizability obeys the following law:[12]

$$\alpha_{\perp}(\omega) = 2\frac{\varepsilon(\omega)-1}{\varepsilon(\omega)+1}, \tag{2}$$

where $L_d=1/2$ and $\varepsilon(\omega)$ is the dielectric function of gold. The parallel polarizability is given by $\alpha_{\parallel}(\omega)=\varepsilon(\omega)-1$. Therefore, the effective dielectric constants are given by[12]

$$\varepsilon_{\text{eff}}^{\perp} = \frac{\varepsilon(\omega)+1+f[\varepsilon(\omega)-1]}{\varepsilon(\omega)+1-f[\varepsilon(\omega)-1]}, \tag{3a}$$

$$\varepsilon_{\text{eff}}^{\parallel} = f\varepsilon(\omega)+(1-f). \tag{3b}$$

The permittivity, $\varepsilon(\omega)$, of the gold film was incorporated by fitting our experimental data with Drude model completed by three Lorentzians. The values of gold permittivity have been extracted from ellipsometric data measured on a flat 90-nm-thick gold deposited at the same conditions as the studied samples. Thus, both the intraband and the interband parts of the dielectric constant were rigorously described. The interband electron transitions between the valence and conduction bands mostly affect the effective refractive indices in the spectral region 250–600 nm. The dielectric function of gold $\varepsilon(\omega)$ was expressed as the sum of Drude and Lorentz terms,

$$\varepsilon(\omega) = \varepsilon_0 - \frac{\omega_p^2}{\omega^2+i\omega\gamma} - \sum_{j=1}^{3}\frac{\Delta\varepsilon_j\Omega_j^2}{\omega^2-\Omega_j^2+i\omega\Gamma_j}. \tag{4}$$

The fitting parameters are $\varepsilon_0=3.9$, $\Delta\varepsilon_j=(0.25,0.5,3.75)$, $\hbar\omega_p=8.97$ eV, $\hbar\gamma=0.03$ eV, $\hbar\Omega_j=(2.68,3.09,4.35)$ eV, and $\hbar\Gamma_j=(0.449,0.845,3)$ eV, where $j=1,2,3$. Figure 7 shows the spectral dependences of the complex refraction index $n+ik=\sqrt{\varepsilon(\omega)}$ for a gold film of thickness 90 nm extracted with ellipsometry (the solid curve) and fitted by expression (4) (the dash-dotted curve). It is worth noting the good agreement between the experimental data and the Drude-Lorentz fit.

Using Eqs. (3a) and (3b) for $\varepsilon_{\text{eff}}^{\perp}$ and $\varepsilon_{\text{eff}}^{\parallel}$, we determined the effective complex refraction index $n_{\text{eff}}^{\perp}+ik_{\text{eff}}^{\perp}$ and $n_{\text{eff}}^{\parallel}+ik_{\text{eff}}^{\parallel}$ which have been used to calculate the optical response of the samples with the help of Fresnel coefficients for the EMA model. The EMA model consisted of air, uniform layer of nanostripes (effective medium), and substrate (glass or bulk gold). Optical response almost does not depend on type of the substrate. Figure 7(b) shows the spectral dependence of the effective optical constants $n_{\text{eff}}^{\perp}$ and $k_{\text{eff}}^{\perp}$, while Fig. 1(c) shows the optical constants $n_{\text{eff}}^{\parallel}$ and $k_{\text{eff}}^{\parallel}$. The dispersion observed for $n_{\text{eff}}^{\perp}$ and $k_{\text{eff}}^{\perp}$ is different from that of the bulk gold. It is easy to check that $n_{\text{eff}}^{\perp}$ and $k_{\text{eff}}^{\perp}$ increase with increasing filling factor f. We note that $n_{\text{eff}}^{\perp}$ and $k_{\text{eff}}^{\perp}$ demonstrate nearly flat bands in the wavelength range (240–500 nm). Note that the characteristic parameter of the effective wave attenuation (or loss ratio) $\gamma=|k_{\text{eff}}^{\perp}/n_{\text{eff}}^{\perp}|$ is less than 1 within all spectral region, with very low number $\gamma\leq 0.3$ in the region blackbody's behaviors. This is in contrast to the pure noble metals which have considerable plasmon losses, $\gamma\geq 1$. It is also worth noting that the effective EMA constants obtained for our structure in the wavelength range of 240–520 nm of blackbody behavior, $n_{\text{eff}}^{\perp}\approx 1.6$ and $k_{\text{eff}}^{\perp}\approx 0.3$, are close to the values of the effective constants which would guarantees the maximal absorption in accordance with the Fresnel coefficients shown in Fig. 1(b). [We should not expect the total coincidence of these effective parameters because the composite deep diffraction gratings studied in our work have been modeled by two layers in the EMA approach and by one layer for the graph in Fig. 1(b).]

The shape of the functions $n_{\text{eff}}^{\parallel}$ and $k_{\text{eff}}^{\parallel}$ is similar to that for a thick gold film [compare to Figs. 7(a) and 7(c)]. Our data [Figs. 7(b) and 7(c)] are consistent with the complex refractive index for homogenous gold layers of surface-relief grating, which produce zero reflectivity, calculated by using a rigorous coupled-wave approach.[24] Note that the difference in the complex refractive indices of effective-medium layer between $n_{\text{eff}}^{\perp}+ik_{\text{eff}}^{\perp}$ and $n_{\text{eff}}^{\parallel}+ik_{\text{eff}}^{\parallel}$ suggests significant optical anisotropy of the gold nanostripes. The measurements of polarized reflection spectra (Figs. 3 and 4) demonstrate explicitly that the gold nanostripes are indeed birefringent. These structures are moderately reflecting for polarization perpendicular to the stripes arrays and highly absorbing for polarization along the arrays. The polarization ratios $|[R_p(\lambda)-R_s(\lambda)]/[R_p(\lambda)+R_s(\lambda)]|$ for the spectral region 250–550 nm are close to 1. Thus, these gold nanostripes could be used as a polarizer over the entire ultraviolet and short wavelength visible spectral region.

To calculate reflectance and transmittance of our system for the azimuth angle $\phi=90°$ we assume that $\varepsilon_p=\varepsilon_{\text{eff}}^{\perp}$ and $\varepsilon_s=\varepsilon_{\text{eff}}^{\parallel}$, while for $\phi=0°$ we take $\varepsilon_s=\varepsilon_{\text{eff}}^{\perp}$ and $\varepsilon_p=\varepsilon_{\text{eff}}^{\parallel}$. The reflectance and transmittance curves were calculated using the Fresnel equations for the three-layer system: air, uniform layer of nanostripes (effective medium), and thick gold (90 nm).[20,21] The only parameters in the calculations are the geometrical sizes of stripes (lattice constant a and width b) and the dielectric constants of gold films, $\varepsilon(\omega)$. We emphasize here that there is no adjustable parameter in these calculations. This makes the agreement of EMA model with experiments even more striking. Figure 7(e) shows the polarized reflection spectra for the case of $\phi=90°$, which are in good qualitative agreement with our experimental data shown in Figs. 3(a) and 3(b). For p-polarized light there are two regions. In the first region, 250–550 nm, the magnitude of $R_p(\lambda)$ is close to zero, and in the second region, 650–1000 nm, the magnitude of $R_p(\lambda)$ tends to one. Figure 7(d) shows that the transmission spectra reaches the maxima at wavelength $\lambda\sim 500$ nm where the reflection $R_p(\lambda)$ drops to minima. We note that extremely low transmission and reflection are consistent with the measured results presented in Figs. 3 and 4.

Figure 7(f) displays the theoretical reflectance from the gold stripes as a function of the wavelength of incident p- and s-polarized light when the incident plane is perpendicular to the arrays direction, $\phi=0°$. The shape and spectral positions of the dips for the reflectivity of s-polarized light [Fig. 5(b)] are well described by our theoretical model [Fig. 7(f)]. It is worth noting that the spectral behaviors of effective complex refraction index $n_{\text{eff}}^{\perp}+ik_{\text{eff}}^{\perp}$ correlate with features in $R_p(\lambda)$ and $T(\lambda)$. Noticeable variations in $n_{\text{eff}}^{\perp}$ and $k_{\text{eff}}^{\perp}$ from optimal values result in the enhancement of $R_p(\lambda)$ and

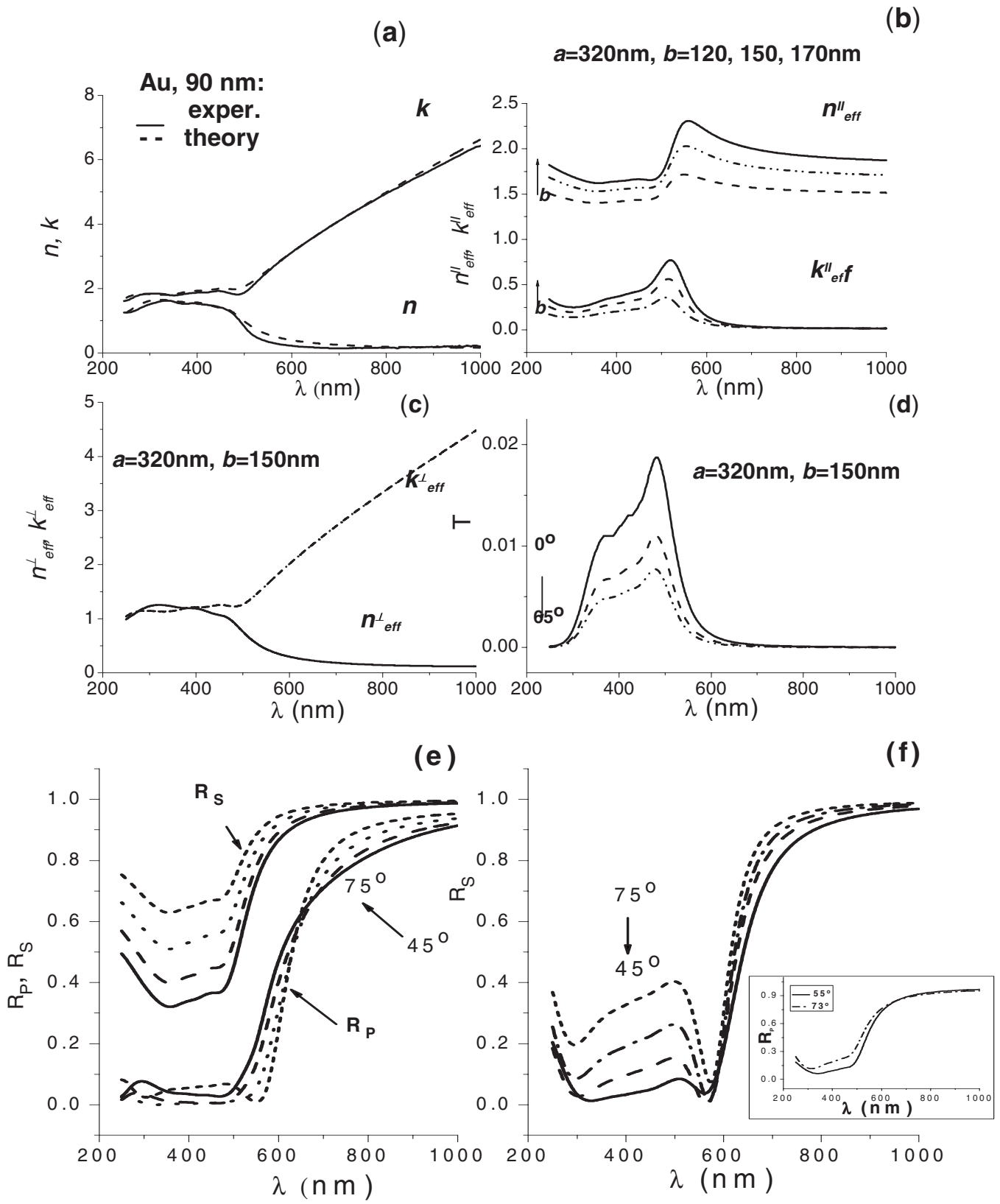

FIG. 7. The effective-medium theory. (a) The complex refraction index for a flat 90 nm gold film as a function of wavelength extracted with ellipsometry (solid line) and theoretical fit (dash-dotted line). (b) The real and imaginary parts of the effective refractive index for the light with the electric field perpendicular to the stripes. (c) The effective refractive index for the light with the electric field parallel to the stripes. (d) The numerical results for transmission spectra for the perpendicular polarization. The theoretical reflection spectra for *p*- and *s*-polarized light for gold nanostripes for case $a=320$ nm and $b=150$ nm calculated for (e) $\phi=90°$ and (f) $\phi=0°$. Inset to (f) shows the theoretical reflection spectra for *p*-polarized light.

$T(\lambda)$. The abrupt change in $R_p(\lambda)$ in the region 500–600 nm can be explained by a drop of $k_{\mathrm{eff}}^{\perp}$ to zero [Fig. 7(b)]. Effective medium exhibits a dielectriclike nature of gold stripes for the region 650–1000 nm in the sense that $n_{\mathrm{eff}}^{\perp} \gg k_{\mathrm{eff}}^{\perp}$.

Physically, the origin of the blackbodylike behavior (total absorption) comes from excitation of localized plasmons in an isolated gold stripe. Due to the negative real part of the dielectric constant of gold $\mathrm{Re}[\varepsilon(\omega)]$ incident light excites localized plasmon resonances.[16–19] These resonances can occur at discrete frequencies and are strongly localized in skin surface layer of stripes. Due to dipole-dipole interaction between ensemble of stripes and strong coupling between localized plasmon, these resonances tend to broaden and produce tight bound bands. The existence of plasmon bands is a necessary condition for creating plasmonic blackbody. The sufficient condition for appearance of almost 100% absorption in our samples is given by a proper choice of the structure parameters of stripes. For noblelike metallic periodical structure the plasma wavelength $\lambda_p = 2\pi\omega_p/c \approx 140$ nm (Au) is a characteristic scale. We have found that the reflection and transmission can be zero when the width of gold stripes is $b \geq \lambda_p$ and exciting plasmon waves can pass through the stripe width completely. It was observed that as b decreases $b < \lambda_p$ the absorption decreases substantially. This is due to the increased reflection at the interface between air and gold stripes.

In order to test our theory further, we calculated the condition for occurrence of the Brewster effect observed for p and s polarizations. EMA predicts the minimum for spectral dependences in $R_p(\lambda)$ [Fig. 7(e)] and $R_s(\lambda)$ [Fig. 7(f)] close to the values observed in experiment [Figs. 3(a) and 5(b)]. Since the effective indices of refraction are different for different configurations of incident plane and direction of stripes arrays, the absence of reflection occurs also at distinguish incident angles for p- and s-polarized light [compare to Figs. 6(a) and 6(c)]. It should be noted that the values of the "Brewster angles" (the angles at which reflection goes to zero) are localized at 50–55° for s-polarized light [Fig. 7(f)] and at 60–65° for p-polarized light and strongly depends on geometrical parameters a and b of measured structures. Our experiments showed that there are zeros in the reflection p- and s-polarized spectra [Figs. 3, 4, 7(e), and 7(f)], which are described well by EMA.

EMA provides a reasonable agreement between the calculated [Figs. 7(e) and 7(f)] and experimental polarization spectra (Figs. 3 and 4). We have also extended our simulation to subwavelength grating based on other metals, namely, Ag and Cu. It was found that the absorption of Cu nanostripes can be at the level of >98% in the wavelengths region 250–500 nm and for broad angles range 0°–75° when the grating parameters are following: the filling factor $f = b/a = 0.5$ and $h = 65$ nm. Near zero-reflectance and transmittance for Ag subwavelength grating can be achieved in the ultraviolet range region (250–400 nm) for the case of grating parameters equal to: the filling factor $f = 0.125$ and $h = 180$ nm. The presented results could be useful as a starting point in subwavelength grating blackbody design optimization.

VI. CONCLUSIONS

We have shown both experimentally and theoretically that composite deep metallic gratings are promising structures for absorptive coatings working in a wide spectral range and for a wide range of incident angles. We demonstrate that plasmonic structures consisting of gold stripes combined with PMMA stripes exhibit almost complete wide-angle absorption over a broad spectral range in visible spectrum important for solar cell operation. We found that polarization and periodicity (grating geometry) play key roles in determining the optical characteristics of the one-dimensional refractory metallic coatings. It was shown that for the gold stripes the reflection totally vanishes for the light with electric vector perpendicular to the stripes in the spectral region 240–550 nm, while the reflection for the other polarization is analogous to that from the plain gold film. We also found that the reflection and transmission spectra in ultraviolet and visible ranges can be controlled by adjusting the width of the gold nanostripes which can be useful for device applications.

We observe the absence of reflection at some angle of incidence (Brewster-type effect) for reflection of both p- and s-polarized waves. Significant birefringence indicates the potential usefulness of a deep metallic subwavelength grating as a reflection polarizer. The reflection and transmission spectra of the gold stripes were interpreted using the effective-medium approximation. This theory confirms blackbodylike behavior and provides satisfactory qualitative description of the optical response of the studied system.

ACKNOWLEDGMENTS

The authors thank Anatoly V. Zayats for fruitful discussions. This work was supported by a Paul Instrument Grant and the EPSRC under Grant No. EP/E01111X/1.

[1] J.-J. Greffet, R. Carminati, K. Joulain, J.-P. Mulet, S. Mainguy, and Y. Chen, Nature (London) **416**, 61 (2002).
[2] C. Luo, A. Narayanaswamy, G. Chen, and J. D. Joannopoulos, Phys. Rev. Lett. **93**, 213905 (2004).
[3] Z. Yu, G. Veronis, S. Fan, and M. L. Brongersma, Appl. Phys. Lett. **89**, 151116 (2006).
[4] D. M. Schaadt, B. Feng, and E. T. Yu, Appl. Phys. Lett. **86**, 063106 (2005).
[5] N. C. Panoiu and R. M. Osgood, Opt. Lett. **32**, 2825 (2007).
[6] D. Derkacs, S. H. Lim, P. Matheu, W. Mar, and E. T. Yu, Appl. Phys. Lett. **89**, 093103 (2006).
[7] G. Kirchhoff, *Ueber den zusammenhang von emission and absorption von licht und warme* (Monatsberichte der Akademie der Wissenschaften, Berlin, 1860), Vol. 1859, p. 783.
[8] M. Planck, *The Theory of Heat Radiation* (Dover, New York, 1959).

[9] A. V. Murphy, B. K. Tsai, and R. D. Saunders, J. Res. Natl. Inst. Stand. Technol. **104**, 487 (1999).
[10] P.-M. Robitaille, IEEE Trans. Plasma Sci. **31**, 1263 (2003).
[11] W. A. de Heer, W. S. Bacsa, A. Chatelain, T. Gerfin, R. Humphrey-Baker, L. Forro, and D. Ugarte, Science **268**, 845 (1995).
[12] F. J. Garcia-Vidal, J. M. Pitarke, and J. B. Pendry, Phys. Rev. Lett. **78**, 4289 (1997).
[13] Zu-Po Yang, L. Ci, J. A. Bur, Sh-Yu Lin, and P. M. Ajayan, Nano Lett. **8**, 446 (2008).
[14] A. N. Grigorenko, A. K. Geim, H. F. Gleeson, Y. Zhang, A. A. Firsov, I. Y. Khrushchev, and J. Petrovic, Nature (London) **438**, 335 (2005).
[15] T. W. Ebbesen, H. L. Lezec, H. F. Ghaemi, T. Thio, and P. A. Wolff, Nature (London) **391**, 667 (1998).
[16] A. V. Zayats and I. I. Smolyaninov, J. Opt. A, Pure Appl. Opt. **5**, S16 (2003).
[17] F. J. Garcia de Abajo, Rev. Mod. Phys. **79**, 1267 (2007).
[18] W.-C. Tan, J. R. Sambles, and T. W. Preist, Phys. Rev. B **61**, 13177 (2000).
[19] M. Kreiter, J. Oster, R. Sambles, S. Herminghaus, S. Mittler-Neher, and W. Knoll, Opt. Commun. **168**, 117 (1999).
[20] R. M. A. Azzam and N. M. Bashara, *Ellipsometry and Polarized Light* (North-Holland, Amsterdam, 1987).
[21] Max Born and E. Wolf, *Principles of Optics* (Cambridge University Press, Cambridge, 1999).
[22] A. Barbara, P. Quemerais, E. Bustarret, and T. Lopez-Rios, Phys. Rev. B **66**, 161403(R) (2002).
[23] A. N. Grigorenko, P. I. Nikitin, and A. V. Kabashin, Appl. Phys. Lett. **75**, 3917 (1999).
[24] T. K. Gaylord, E. N. Glytsis, and M. G. Moharam, Appl. Opt. **26**, 3123 (1987).
[25] M. G. Moharam and T. K. Gaylord, J. Opt. Soc. Am. A **3**, 1780 (1986).
[26] L. B. Mashev, E. Popov, and E. G. Loewen, Appl. Opt. **28**, 2538 (1989).
[27] F. J. Garcia-Vidal, J. Sanchez-Dehesa, A. Dechelette, E. Bustarret, T. Lopez-Rios, T. Fournier, and B. Pannetier, J. Lightwave Technol. **17**, 2191 (1999).
[28] F. J. Garcia-Vidal, L. Martin-Moreno, and J. B. Pendry, J. Opt. A, Pure Appl. Opt. **7**, S97 (2005).
[29] F. J. Garcia-Vidal and L. Martin-Moreno, Phys. Rev. B **66**, 155412 (2002).
[30] R. Gomez-Medina, Opt. Express **14**, 3730 (2006).
[31] J. C. M. Garnett, Philos. Trans. R. Soc. London, Ser. A **203**, 385 (1904).